nature nanotechnology

LETTERS

https://doi.org/10.1038/s41565-021-00953-w

Check for updates

Complete structural characterization of single carbon nanotubes by Rayleigh scattering circular dichroism

Fengrui Yao[1,11], Wentao Yu[1,11], Can Liu[1,11], Yingze Su[1], Yilong You[1], He Ma[1], Ruixi Qiao[2], Chunchun Wu[1], Chaojie Ma[1], Peng Gao[2], Fajun Xiao[3], Jianlin Zhao[3], Xuedong Bai[4,5], Zhipei Sun[6], Shigeo Maruyama[7], Feng Wang[8], Jin Zhang[9] and Kaihui Liu[1,2,5,10] ✉

Non-invasive, high-throughput spectroscopic techniques can identify chiral indices (*n*,*m*) of carbon nanotubes down to the single-tube level[1–6]. Yet, for complete characterization and to unlock full functionality, the handedness, the structural property associated with mirror symmetry breaking, also needs to be identified accurately and efficiently[7–14]. So far, optical methods fail in the handedness characterization of single nanotubes because of the extremely weak chiroptical signals (roughly 10^{-7}) compared with the excitation light[15,16]. Here we demonstrate the complete structure identification of single nanotubes in terms of both chiral indices and handedness by Rayleigh scattering circular dichroism. Our method is based on the background-free feature of Rayleigh scattering collected at an oblique angle, which enhances the nanotube's chiroptical signal by three to four orders of magnitude compared with conventional absorption circular dichroism. We measured a total of 30 single-walled carbon nanotubes including both semiconducting and metallic nanotubes and found that their absolute chiroptical signals show a distinct structure dependence, which can be qualitatively understood through tight-binding calculations. Our strategy enables the exploration of handedness-related functionality of single nanotubes and provides a facile platform for chiral discrimination and chiral device exploration at the level of individual nanomaterials.

Carbon nanotubes, the prototypical one-dimensional material, are generally chiral except for zigzag and armchair nanotubes (Fig. 1a and Supplementary Fig. 1). Two nanotube enantiomers, left- and right-handed, can show different interactions with circularly polarized light (Fig. 1b). From a fundamental point of view, when excited by an external field **E**, both the electric moment **μ** and the magnetic moment **m** exist in chiral nanotubes (in achiral nanotubes, $m=0$). Quantitatively, **m** is defined as $i\mathbf{GE}$, where **G** is the complex electric-magnetic coupled susceptibility and its imaginary part (G_2) is related to the chiral asymmetry of the material[17,18]. Since the orientation of **m** (determined by the sign of G_2) varies with the nanotube handedness, in principle, it is possible to identify the nanotube handedness through circular dichroic spectroscopic techniques (Supplementary Note 1). So far, several circular dichroism spectroscopic techniques have been successfully established[19–22], and can measure the chiral optical response of single chiral plasmonic nanostructures and nanoparticles[23–25]. However, when these techniques are applied to a single carbon nanotube, great difficulties are encountered due to the interference of circularly polarized light distortion[26], chiral experimental arrangements[27,28] or the sample substrate[29]. Currently, only non-optical techniques, such as scanning tunnelling microscopy and transmission electron microscopy, can be used for handedness identification of individual carbon nanotubes[30,31], whereas they have proved to be unsuitable for scalable and routine characterization due to their limited accessibility and low efficiency.

To alleviate this dilemma, we experimentally develop a high-sensitivity Rayleigh scattering circular dichroism spectroscopic technique. As shown in Fig. 1c, a supercontinuum laser coupled with a tunable filter provides broadband excitation light with variable wavelength λ, a polarizer and a photoelastic modulator (PEM) are used to generate alternating left- and right-handed circularly polarized light with a frequency of 50 kHz, a polarization-maintaining objective serves to focus the modulated light onto nanotubes and an obliquely placed objective is used to collect the nanotube-scattering light (Supplementary Fig. 2). Since the intensity of the nanotube scattering varies with the polarization of the incident light, the detected intensity includes a time-varying signal (I_{AC}) at the alternating frequency (f) of the circularly polarized light and an average signal (I_{DC}) (Fig. 1d and Supplementary Note 2). Experimentally, the time-varying value is recorded by a lock-in amplifier, and the average Rayleigh scattering intensity is read from a photomultiplier tube simultaneously (see Methods for more details). The Rayleigh scattering circular dichroism (Ray-CD) intensity at a wavelength (λ) can be finally obtained as

[1]State Key Laboratory for Mesoscopic Physics, Frontiers Science Center for Nano-optoelectronics, School of Physics, Peking University, Beijing, China. [2]International Center for Quantum Materials, Collaborative Innovation Center of Quantum Matter, Peking University, Beijing, China. [3]Shanxi Key Laboratory of Optical Information Technology, School of Physical Science and Technology, Northwestern Polytechnical University, Xi'an, China. [4]Beijing National Laboratory for Condensed Matter Physics, Institute of Physics, Chinese Academy of Sciences, Beijing, China. [5]Songshan Lake Materials Laboratory, Institute of Physics, Chinese Academy of Sciences, Dongguan, China. [6]Department of Electronics and Nanoengineering, QTF Center of Excellence, Aalto University, Espoo, Finland. [7]Department of Mechanical Engineering, The University of Tokyo, Tokyo, Japan. [8]Department of Physics, University of California at Berkeley, Berkeley, CA, USA. [9]Center for Nanochemistry, College of Chemistry and Molecular Engineering, Peking University, Beijing, China. [10]Interdisciplinary Institute of Light-Element Quantum Materials and Research Center for Light-Element Advanced Materials, Peking University, Beijing, China. [11]These authors contributed equally: Fengrui Yao, Wentao Yu, Can Liu. ✉e-mail: khliu@pku.edu.cn

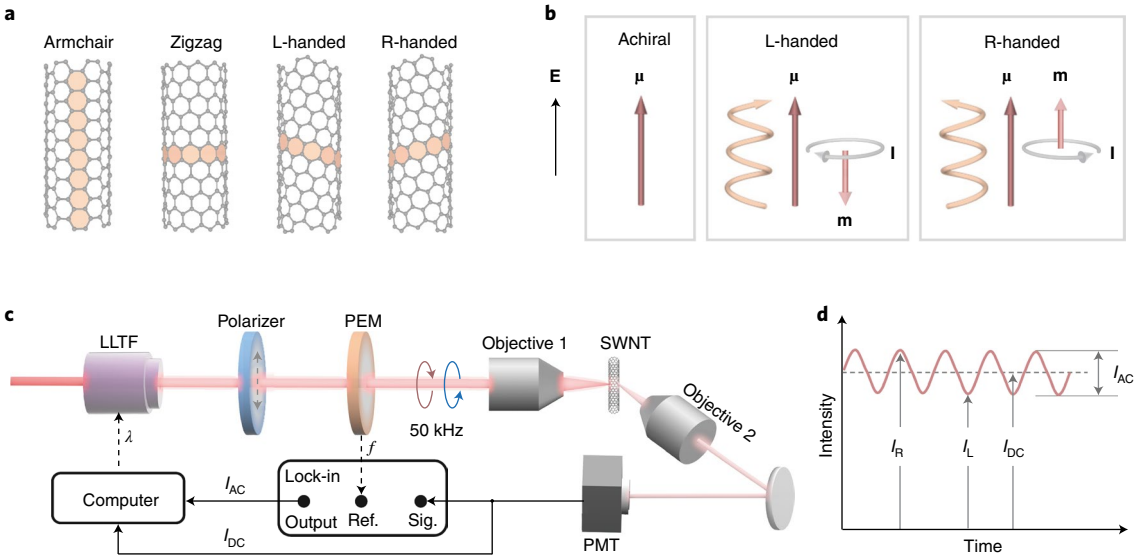

Fig. 1 | Chiroptical signal measurement for single nanotubes. a, Schematic geometric structure of carbon nanotubes with different helicities, where zigzag chains are highlighted for clarity. L-handed (R-handed) represents nanotubes with left-handedness (right-handedness). **b**, Different optical responses to circularly polarized light of nanotubes with different chiral asymmetries. When excited by an external field **E**, an electric moment **μ** is excited both in achiral and chiral nanotubes, whereas a circular current **I** and magnetic moment **m** are excited only in chiral nanotubes and their directions are reversed with a change in nanotube handedness, making them distinguishable in chiroptical experiments. **c**, Schematic of the Ray-CD experimental setup, showing the placement of optical components and connection of electronic instruments. LLTF, laser line tunable optical filter; PMT, photomultiplier tube. **d**, Simplified diagram of the nanotube-scattering intensity over time, containing the average signal (I_{DC}) and signal varying with the alternating circularly polarized incident light (I_{AC}).

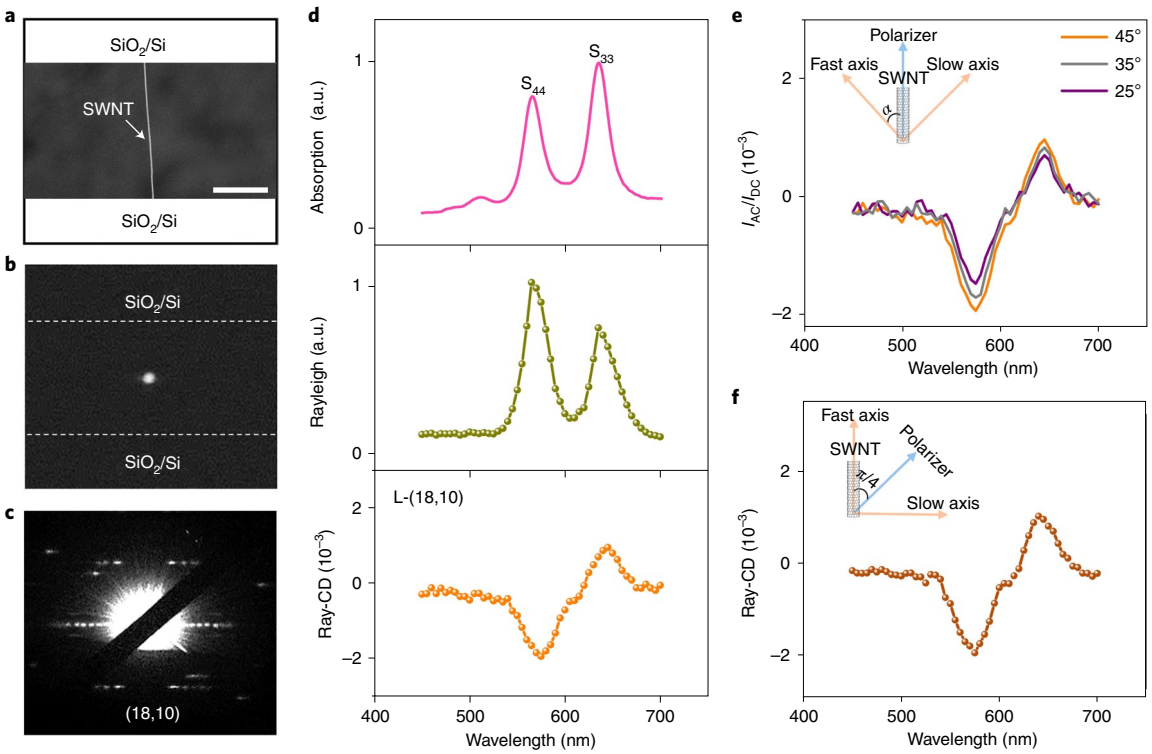

Fig. 2 | Rayleigh circular dichroism measurement for a suspended nanotube. a, Scanning electron microscopy image of a suspended single-walled nanotube across an open slit. Scale bar, 10 μm. **b**, Rayleigh scattering image of the nanotube (the bright spot in the slit centre). Edges of the slit are marked with white dashed lines. **c**, Transmission electron microscopic diffraction image of the nanotube; on the basis of this image, the nanotube was identified to have a chiral index of (18,10) and to be a semiconducting type I nanotube. **d**, Optical absorption spectrum (top), Rayleigh scattering spectrum (middle) and Ray-CD spectrum (bottom) for the nanotube. On the basis of the signs of the two optical transitions in the Ray-CD spectrum and its type I category, left-handedness was determined. a.u., arbitrary units. **e**, A set of modulated signals (I_{AC}/I_{DC}) measured at different angle (α) values, showing the declining modulated signals for the one-dimensional nanotubes as α decreases from 45° to 25°. **f**, Ray-CD spectra measured after rotating both the polarizer and the fast axis of PEM crystal $\pi/4$, which show no obvious changes, proving the low interference from the linear dichroism and linear birefringence effects. The inset in **e** and **f** shows the layouts for polarization control and the nanotube.

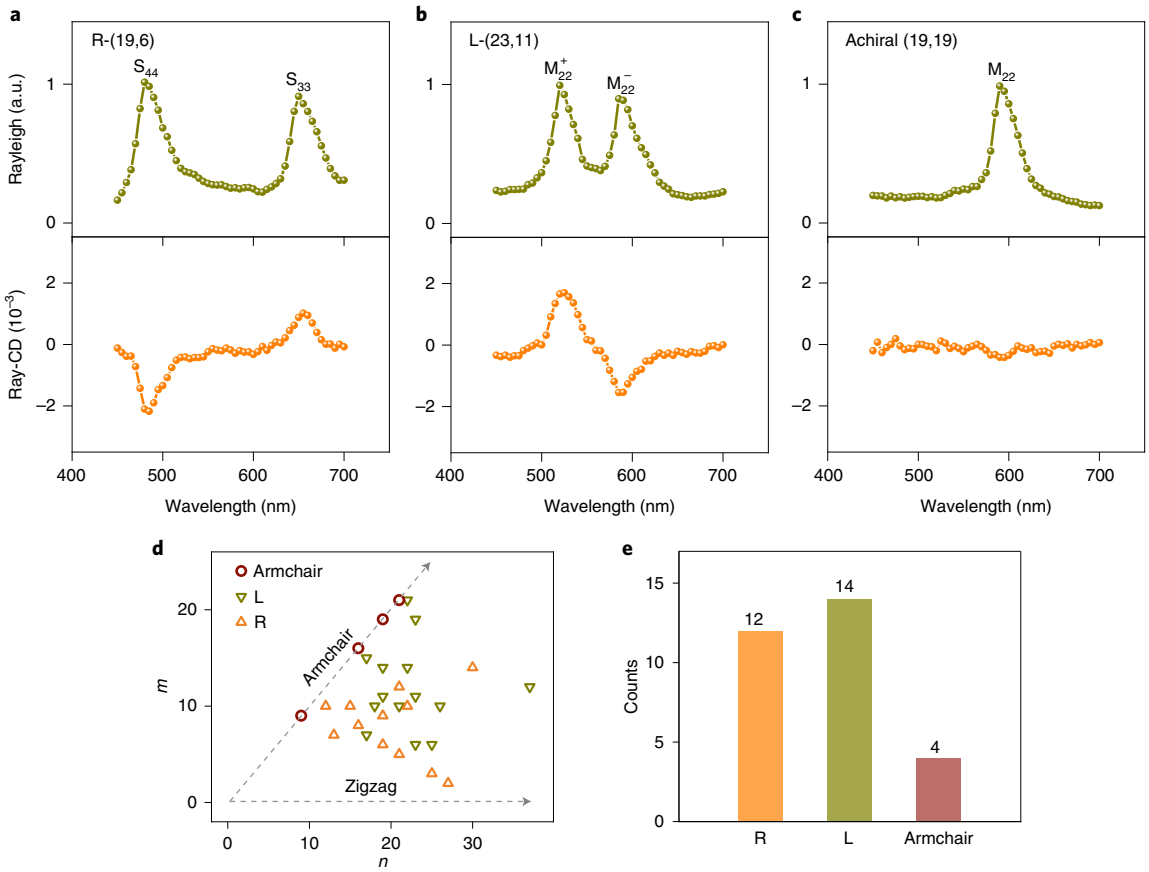

Fig. 3 | Typical Ray-CD results for three representative nanotubes and the summary of handedness results for 30 nanotubes. a–c, Rayleigh scattering (top) and Ray-CD (bottom) spectra for semiconducting (19,6) (**a**), chiral metallic (23,11) (**b**) and armchair (19,19) (**c**) nanotubes. Optical transitions are marked above each peak, which were used to determine the chiral indices of the nanotubes. Furthermore, the nanotube handedness was identified from the signs of the Ray-CD peaks and their type category. **d**, Detailed chiral index and handedness distribution for 30 measured nanotubes. The nanotubes were grown with iron catalysts. **e**, Histogram for the handedness distribution, showing similar proportions of left- and right-handed nanotubes.

$$I_{\mathrm{RCD}}(\lambda) = \frac{(I_{\mathrm{L}} - I_{\mathrm{R}})}{(I_{\mathrm{L}} + I_{\mathrm{R}})} = \frac{I_{\mathrm{AC}}}{I_{\mathrm{DC}}} \times A,$$

where I_{L} (I_{R}) represents the Rayleigh scattering intensity excited by left-handed (right-handed) circularly polarized light, and A is an experimental constant (Supplementary Note 2). As the laser wavelength is swept from 450 to 700 nm, the Rayleigh scattering and Ray-CD spectra can be obtained simultaneously. In our measurement, to obtain a high purity for the light polarization, the PEM has been precisely calibrated (Supplementary Fig. 3 and Supplementary Note 3), and all optical components with minimized residual birefringence have been carefully selected by monitoring the destruction of the extinction ratio when placing them between two crossed polarizers. Meanwhile, we used a spatial filter unit to obtain a focused Gaussian beam (Supplementary Fig. 4) and guaranteed that the light passed perpendicularly through the centre of the optical components, which is critically required to realize the Ray-CD measurements.

We first applied this technique to an isolated semiconducting single-walled carbon nanotube (SWNT) (Fig. 2a), which was directly grown over the slit structure by chemical vapour deposition (see Methods and Extended Data Fig. 1 for details). The scattering light of the nanotube can be focused and seen in the Rayleigh image (the bright spot in the slit centre), by which the spatial position of the nanotube relative to the laser focus can be monitored in real time (Fig. 2b). The chiral index of the nanotube was unambiguously determined as (18,10) from its electron diffraction pattern (Fig. 2c) and the two prominent optical resonances in its absorption (Fig. 2d, top) or Rayleigh spectrum[4] (Fig. 2d, middle). According to the type definition of carbon nanotubes (for type I, $|n-m|$ mod $3=2$; for type II, $|n-m|$ mod $3=1$, where mod represents the modulo operation), we can determine that this nanotube belongs to type I. In addition, according to the established atlas for SWNT optical transitions[4], the two resonance peaks at approximately 565 and 635 nm were assigned to the S_{44} and S_{33} optical transitions of the nanotube (18,10), respectively. In contrast to the absorption spectrum, the Rayleigh peaks show different line shapes and a slight redshift due to the influence of the real part of the complex optical susceptibility, which is consistent with the previous report[2].

In particular, the acquired Ray-CD spectrum (Fig. 2d, bottom) also possesses two appreciable peaks at positions similar to those observed in the absorption and Rayleigh spectra but with opposite signs, which provides handedness information for this nanotube. Such opposite signs of neighbouring transitions can be understood in the cutting-line concept of nanotube optical transitions. For neighbouring transitions, their corresponding cutting lines are located on the opposite side of the K point of the Brillouin zone in a zone-folding scheme (Supplementary Fig. 5), thus resulting in the opposite wave vectors (k) of the electron and magnetic dipole moments of the transition[32]. In such cases, alternating signs for the neighbouring Ray-CD signal at van Hove singular energies ($\mathbf{E}_{ii}$, $i=1$, 2, 3, 4, 5, …) are expected. In addition, owing to the difference in the cutting lines between semiconducting type I and type II nanotubes,

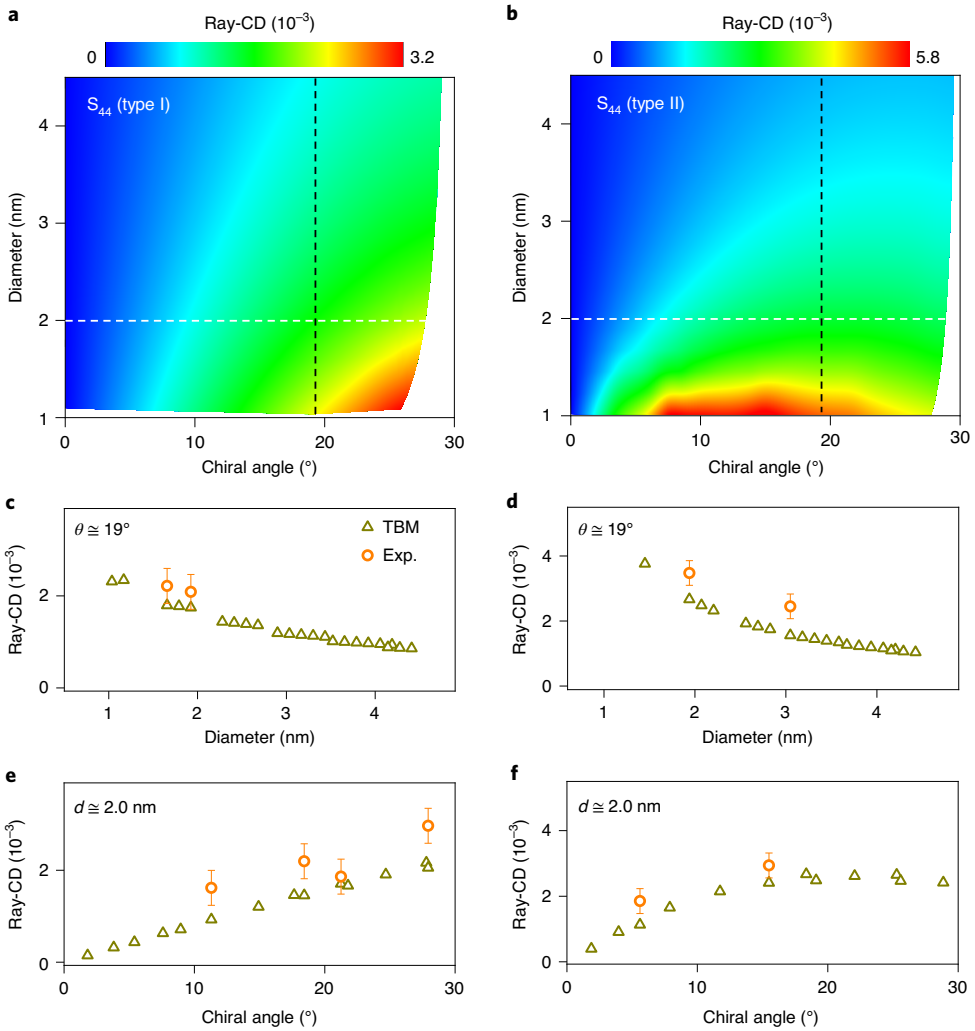

Fig. 4 | Structure-dependent Ray-CD peak intensity. a,**b**, Calculated mapping based on the tight-binding model (TBM) of the Ray-CD peak intensity as a function of the diameter and chiral angle of the S_{44} transition for semiconducting type I (**a**) and type II (**b**) nanotubes. **c**,**d**, Calculated (green triangles) versus experimental (orange circles) peak Ray-CD intensities for S_{44} transitions as a function of diameter for the type I (**c**) and type II (**d**) families. The chiral angle of the selected nanotubes is approximately 19° (black lines in the calculated mappings). **e**,**f**, Calculated (green triangles) versus experimental (orange circles) peak Ray-CD intensities for S_{44} transitions as a function of chiral angle for type I (**e**) and type II (**f**) families. The diameter of the selected nanotubes was approximately 2 nm (white lines in the calculated mappings). Error bars are derived from the absolute values obtained for armchair nanotubes (see Methods for more details).

the given transition for type I and type II nanotubes will have opposite signs (Supplementary Fig. 5). As a result, for left-handed type I nanotubes (type II nanotubes), odd (even) transitions should have positive signs, while the opposite is true for the case of right-handed nanotubes[7,13,15]. Accordingly, the nanotube (18,10) measured here was identified as left-handed on the basis of the positive Ray-CD sign of the S_{33} transitions and its type I category.

In addition to the sign information, one can clearly see that the magnitude of the Ray-CD peak signal is as large as 10^{-3}, which is approximately four orders of magnitude larger than that in the absorption circular dichroism (predicted as roughly 10^{-7})[15], illustrating the high sensitivity of our technique. In contrast, the signal is nearly zero when the nanotube is moved out of the laser spot, confirming that there is little spurious signal in the Rayleigh measurement (Supplementary Fig. 6). Furthermore, we proved that the obtained Ray-CD signal indeed originates from the nanotube itself by changing the polarization of the excitation light. According to calculations (Supplementary Note 4), when reducing the angle (α) between the optical axis of the PEM and polarizer (Fig. 2e inset), the excitation light can be modulated between left- and right-handed elliptically polarized light instead of circularly polarized light; thus, the modulated signal (I_{AC}/I_{DC}) of the one-dimensional nanotube should decrease with α. As expected, a declining trend was observed experimentally as α changed from 45° to 25° (Fig. 2e). In addition, we rotated both the polarizer and the fast axis of PEM crystal $\pi/4$ while keeping the axis of the nanotube and the angle between the polarizer and the fast axis of the PEM unchanged (Fig. 2f inset). As a result, no obvious changes in the Ray-CD spectra were observed (Fig. 2f), which proved the low contribution from linear birefringence and linear dichroism effects (Supplementary Note 5)[33,34].

To further investigate the chiral behaviour of SWNTs, we performed measurements for different semiconducting and metallic nanotubes, three of which were displayed representatively. Their chiral indices were first determined by the resonance peaks in the absorption (Supplementary Fig. 7) or Rayleigh spectrum (Fig. 3a–c, top), and their handedness was subsequently identified

by the corresponding signs of the Ray-CD signals (Fig. 3a–c, bottom). Distinct from the type I nanotube (18,10), although both signs for the Ray-CD signals for the S_{44} and S_{33} transitions (Fig. 3a) are the same as those shown in Fig. 2d, the handedness of this type II nanotube (19,6) was identified as right rather than left. In addition, an example of a chiral metallic nanotube (23,11) is displayed in Fig. 3b, where M_{22}^{+} and M_{22}^{-} transitions split by the trigonal warping effect and the corresponding Ray-CD signals with opposite signs can be observed, in line with previous theoretical expectations[13]. Similar to semiconducting nanotubes, the M_{ii}^{-} transitions should have positive (negative) signs for right-handed (left-handed) metallic nanotubes[13]; hence, this metallic nanotube was determined to be left-handed on the basis of the experimental Ray-CD spectrum. Besides, the non-peak feature of the Ray-CD spectrum of the armchair nanotube (19,19) proved the acceptable introduced noise in our experiment (Fig. 3c, bottom).

The ability to measure chiroptical signals at the single-tube level allows us to investigate the structure-dependent chiral properties of nanotubes. In this work, we systematically measured a total of 30 single nanotubes and found that their absolute Ray-CD signals at the resonance peaks varied in the range of 1×10^{-3} to 4×10^{-3}. Theoretically, we calculated the Ray-CD peak intensity based on a tight-binding method[13] and time-dependent perturbation theory[17,18] (Supplementary Note 6). Ray-CD amplitudes for S_{44} optical transitions were calculated, and the colour maps for semiconducting type I and type II nanotubes with diameters ranging between 1.0 and 4.5 nm are plotted in Fig. 4a,b, respectively. The general trend shows that the larger nanotubes have smaller signals. A simple understanding is that the larger nanotubes have surfaces that are less curved, so the chiral effects are less intense. In the limiting case, when the diameter goes to infinity and recovers the monolayer hexagonal graphene sheet, the Ray-CD will be zero[15]. In addition, it is evident that the Ray-CD peak intensities for the type I and II nanotubes manifest different chiral angle dependences. For nanotubes with large diameters ($d>2.0$ nm), the Ray-CD intensity of both type I and type II nanotubes is increased when the chiral angle enlarges. However, for nanotubes with relatively small diameters ($d<2.0$ nm), type II nanotubes exhibit non-monotonic behaviour with chiral angle. Additionally, such type-dependent asymmetry is reversed for S_{33} optical transitions (Extended Data Fig. 2). All these phenomena can be correlated with the anisotropic energy bands of the nanotubes, whereby equienergy contours in the Brillouin zone of graphene evolve from circles around the K point to triangular shapes around the M point, and the energy dispersion is different on the two sides of the K point[32]. For nanotubes with smaller diameters, their optical transitions have larger energy, and the corresponding cutting lines are far away from the K point; therefore, the Ray-CD patterns show larger asymmetry between type I and type II nanotubes.

Next, we present a comparison between the theoretical prediction (green triangles) and experimental data (orange circles) for nanotubes with approximately the same chiral angle ($\theta\cong19°$, Fig. 4c,d) and same diameter ($d\cong2.0$ nm, Fig. 4e,f). The experimental data show the same trend as the calculated data, while deviations are observed and might be ascribed to the many-body excitonic effects beyond the tight-binding models[13] (Supplementary Note 6), as well as the higher-order effects of multipole expansion in the time-dependent perturbation theory[17,18] (Supplementary Note 1).

Accurate and facile characterization can be an indispensable tool for the handedness-controlled growth of carbon nanotubes. Here, we summarize the chiral indices and handedness distributions for the 30 single nanotubes measured (Fig. 3d and Supplementary Tables 1 and 2) and plot a histogram for armchair, left- and right-handed nanotubes (Fig. 3e), whereas no obvious handedness priority was found under our growth conditions with iron catalysts[35] (see growth details in Methods). This randomness in the handedness may arise from the fact that iron catalysts are in the liquid phase at the growth temperature of approximately 950 °C. In the future, solid catalysts with asymmetric surfaces can be used to grow nanotubes with preferred or even pure handedness, and our method can provide key feedbacks. Such chiral-sensitive measurements also allow one to explore the influence of handedness on the coupling of double-walled carbon nanotubes or the coupling of other one-dimensional van der Waals heterostructures[36]. This will certainly facilitate their fundamental investigations and practical applications ranging from electronic circuits, photonic and optoelectronic devices. This new methodology may fill the vacancy of full handedness discrimination at the individual nanotube scale, and can be universal for characterizing the chiral properties of other single nanomaterials, therefore offering a facile platform for the exploration of low-dimensional chiral physics and chiral devices.

Online content

Any methods, additional references, Nature Research reporting summaries, source data, extended data, supplementary information, acknowledgements, peer review information; details of author contributions and competing interests; and statements of data and code availability are available at https://doi.org/10.1038/s41565-021-00953-w.

Received: 1 September 2020; Accepted: 5 July 2021;
Published online: 12 August 2021

References

1. Bachilo, S. M. et al. Structure-assigned optical spectra of single-walled carbon nanotubes. *Science* **298**, 2361–2366 (2002).
2. Sfeir, M. Y. et al. Probing electronic transitions in individual carbon nanotubes by Rayleigh scattering. *Science* **306**, 1540–1543 (2004).
3. Dresselhaus, M. S., Dresselhaus, G., Saito, R. & Jorio, A. Raman spectroscopy of carbon nanotubes. *Phys. Rep.* **409**, 47–99 (2005).
4. Liu, K. et al. An atlas of carbon nanotube optical transitions. *Nat. Nanotechnol.* **7**, 325–329 (2012).
5. Liu, K. et al. High-throughput optical imaging and spectroscopy of individual carbon nanotubes in devices. *Nat. Nanotechnol.* **8**, 917–922 (2013).
6. Liu, K. H. et al. Systematic determination of absolute absorption cross-section of individual carbon nanotubes. *Proc. Natl Acad. Sci. USA* **111**, 7564–7569 (2014).
7. Samsonidze, G. G. et al. Interband optical transitions in left- and right-handed single-wall carbon nanotubes. *Phys. Rev. B* **69**, 205402 (2004).
8. Peng, X. et al. Optically active single-walled carbon nanotubes. *Nat. Nanotechnol.* **2**, 361–365 (2007).
9. Ghosh, S., Bachilo, S. M. & Weisman, R. B. Advanced sorting of single-walled carbon nanotubes by nonlinear density-gradient ultracentrifugation. *Nat. Nanotechnol.* **5**, 443–450 (2010).
10. Wei, X. et al. Experimental determination of excitonic band structures of single-walled carbon nanotubes using circular dichroism spectra. *Nat. Commun.* **7**, 12899 (2016).
11. Ao, G., Streit, J. K., Fagan, J. A. & Zheng, M. Differentiating left- and right-handed carbon nanotubes by DNA. *J. Am. Chem. Soc.* **138**, 16677–16685 (2016).
12. Magg, M. et al. Resonance raman optical activity spectra of single-walled carbon nanotube enantiomers. *J. Phys. Chem. Lett.* **7**, 221–225 (2016).
13. Sato, N., Tatsumi, Y. & Saito, R. Circular dichroism of single-wall carbon nanotubes. *Phys. Rev. B* **95**, 155436 (2017).
14. Brandt, J. R., Salerno, F. & Fuchter, M. J. The added value of small-molecule chirality in technological applications. *Nat. Rev. Chem.* **1**, 0045 (2017).
15. Sanchez-Castillo, A., Roman-Velazquez, C. E. & Noguez, C. Optical circular dichroism of single-wall carbon nanotubes. *Phys. Rev. B* **73**, 045401 (2006).
16. Barron, L. D. *Molecular Light Scattering and Optical Activity* (Cambridge Univ. Press, 2009).
17. Tang, Y. & Cohen, A. E. Optical chirality and its interaction with matter. *Phys. Rev. Lett.* **104**, 163901 (2010).
18. Yang, N. & Cohen, A. E. Local geometry of electromagnetic fields and its role in molecular multipole transitions. *J. Phys. Chem. B* **115**, 5304–5311 (2011).
19. Sioncke, S., Verbiest, T. & Persoons, A. Second-order nonlinear optical properties of chiral materials. *Mater. Sci. Eng. R. Rep.* **42**, 115–155 (2003).
20. Fischer, P. & Hache, F. Nonlinear optical spectroscopy of chiral molecules. *Chirality* **17**, 421–437 (2005).
21. Persoons, A. Nonlinear optics, chirality, magneto-optics: a serendipitous road. *Opt. Mater. Express* **1**, 5–16 (2011).
22. Collins, J. T. et al. Chirality and chiroptical effects in metal nanostructures: fundamentals and current trends. *Adv. Opt. Mater.* **5**, 1700182 (2017).

23. Collins, J. et al. First observation of optical activity in hyper-Rayleigh scattering. *Phys. Rev. X.* **9**, 011024 (2019).
24. Sachs, J., Gunther, J. P., Mark, A. G. & Fischer, P. Chiroptical spectroscopy of a freely diffusing single nanoparticle. *Nat. Commun.* **11**, 4513 (2020).
25. Ohnoutek, L. et al. Single nanoparticle chiroptics in a liquid: optical activity in hyper-Rayleigh scattering from Au helicoids. *Nano Lett.* **20**, 5792–5798 (2020).
26. Tang, Y., Cook, T. A. & Cohen, A. E. Limits on fluorescence detected circular dichroism of single helicene molecules. *J. Phys. Chem. A* **113**, 6213–6216 (2009).
27. Westphal, C., Bansmann, J., Getzlaff, M. & Schonhense, G. Circular dichroism in the angular distribution of photoelectrons from oriented CO molecules. *Phys. Rev. Lett.* **63**, 151–154 (1989).
28. Verbiest, T., Kauranen, M., Van Rompaey, Y. & Persoons, A. Optical activity of anisotropic achiral surfaces. *Phys. Rev. Lett.* **77**, 1456 (1996).
29. Yokoyama, A., Yoshida, M., Ishii, A. & Kato, Y. K. Giant circular dichroism in individual carbon nanotubes induced by extrinsic chirality. *Phys. Rev. X* **4**, 011005 (2014).
30. Odom, T. W., Huang, J.-L., Kim, P. & Lieber, C. M. Atomic structure and electronic properties of single-walled carbon nanotubes. *Nature* **391**, 62 (1998).
31. Liu, Z. et al. Determination of optical isomers for left-handed or right-handed chiral double-wall carbon nanotubes. *Phys. Rev. Lett.* **95**, 187406 (2005).
32. Saito, R., Dresselhaus, G. & Dresselhaus, M. Trigonal warping effect of carbon nanotubes. *Phys. Rev. B* **61**, 2981 (2000).
33. Shindo, Y., Nakagawa, M. & Ohmi, Y. On the problems of CD spectropolarimeters. II: artifacts in CD spectrometers. *Appl. Spectrosc.* **39**, 860–868 (1985).
34. Kuroda, R., Harada, T. & Shindo, Y. A solid-state dedicated circular dichroism spectrophotometer: development and application. *Rev. Sci. Instrum.* **72**, 3802–3810 (2001).
35. He, M., Zhang, S. & Zhang, J. Horizontal single-walled carbon nanotube arrays: controlled synthesis, characterizations, and applications. *Chem. Rev.* **120**, 12592–12684 (2020).
36. Xiang, R. et al. One-dimensional van der Waals heterostructures. *Science* **367**, 537–542 (2020).

Methods

Sample preparation. Suspended SWNTs were grown across slit structures by the chemical vapour deposition method (Extended Data Fig. 2). The slit structures (30 μm × 1 mm) were prepared by standard photolithography and wet etching techniques. A thin iron film (0.2 nm) was deposited as the catalyst at one end of the silicon substrate, which was then loaded into the quartz tube (1 inch) of the chemical vapour deposition furnace. The system was heated to 950 °C in 30 min with 300 standard cubic centimetres per minute (sccm) Ar and 200 sccm H_2. When the growth temperature reached, ethanol vapour through a bubbler with 100 sccm Ar was introduced as the carbon precursor for SWNTs growth. Since the growth of SWNTs follows the kite-flying mechanism directed by the gas flow in this condition, long SWNTs could grow across the open slit on the substrates[35].

Transmission and scanning electron microscopy characterization. Electron diffraction patterns were obtained by a transmission electron microscope (JEOL 2100 and ARM 3000) under 80 keV. Both the electron beam and laser beam can go through the open slit with individual carbon nanotubes, which enables direct measurement of diffraction patterns and optical spectra of the same nanotube. Scanning electron microscopy images were collected by Hitachi S-4800 field emission at 5 kV.

Ray-CD measurements. A laser line filter (NKT) was used to select monochromatic light from the coupled supercontinuum laser (NKT, WL-SC-400-4) consecutively. A spatial filter unit was used to get a good Gaussian beam. At each wavelength, alternating left- and right-handed circularly polarized lights (50 kHz switching frequency) were generated with a polarizer (Thorlabs, GTH10M) and PEM (Hinds, PEM100). One objective (Mitutoyo M Plan ×50, numerical aperture (NA) = 0.25) was served to focus the light on suspended nanotubes, and another oblique objective (Mitutoyo M Plan ×20, NA = 0.25) was used to collect the nanotube-scattering signal (Supplementary Fig. 8). A pair of confocal lenses (Thorlabs, AC254-050-A-ML) and a pinhole (Thorlabs, P200D) were used to filter stray scattering before the signal reaching the detector (Thorlabs, PMT2001). To monitor the position of carbon nanotubes, a flip mirror was used to switch the scattering light to a CCD camera (PULNIX, TM-7CN) for Rayleigh scattering imaging. The effective value and sign of the time-varying signal (I_{AC}) changed with the incident circularly light, and was extracted by a lock-in amplifier (Stanford Research, SR-830) referenced to the modulated frequency of PEM. At the same time, a high-speed data acquisition card (National Instruments, PCI-6289) connected to a computer was used to record the average scattering signal (I_{DC}). Finally, the Ray-CD (RCD) signal (I_{RCD}) at the wavelength of λ was obtained as $I_{RCD}(\lambda) = \frac{I_{AC}}{I_{DC}} \times A$, where A is an experimental constant. The monochromatic light selection, PEM retardance adjustment and data acquisition were controlled by the same computer. As the laser wavelength scanned the whole spectral range (450 to 700 nm, 5 nm increments), both Rayleigh scattering and Ray-CD spectra of a SWNT were obtained after being normalized by the detected profile of the supercontinuum light (Supplementary Fig. 9). The handedness determination of the carbon nanotube was based on the sign of Ray-CD spectra at specific optical transitions and was furtherly confirmed by the scanning tunnelling microscopic image of the same nanotube (Supplementary Fig. 10). In addition, to make the nanotube axis perpendicular to the incident light for avoiding spurious signals from the experimental setup (Supplementary Note 7), we used a sample holder with two-axis adjusters (Thorlabs PY003/M) to control the sample tilt within 50 μrad. To characterize the noise of the system, Ray-CD spectra of four armchair SWNTs with different resonance positions were measured and their corresponding peak intensities were recorded (Supplementary Fig. 11). In practice, we took average of absolute values of four armchair tubes as the error bar (3.8×10^{-4}) of Ray-CD values for other chiral nanotubes.

Absorption measurements. The absorption spectra of nanotubes were obtained using the polarization-based transmission microscopy developed previously[6]. In detail, a supercontinuum laser (Fianium SC-400-4) provided a wide-band light source, then the light propagated through polarizer 1 (Thorlabs, GTH10M) and was focused on the sample by objective 1 (Mitutoyo ×50, NA = 0.25). The transmitted light was collected by another confocal objective 2 (Mitutoyo ×50, NA = 0.42). Polarizer 2 was placed with a relative angle of roughly 90° with polarizer 1 (with δ deviation), and the nanotubes were placed with their axis 45° to polarizer 1. Two sets of spectra with the nanotube in and out of the beam focus were obtained to generate the contrast signal detected by a spectrometer containing a grating. On the basis of the extinction signal measured at opposite deviation angles ($\pm\delta$), the absorption spectra for the single carbon nanotube can be further obtained. In addition, this instrument was coupled to the Ray-CD experiment setup, allowing both measurements of absorption and Ray-CD spectra on the same nanotube. All the optical measurements were done in the cleanroom where the temperature was kept constant at roughly 20 °C.

Data availability

The data supporting the findings of this study are available within the paper, Extended Data Figs. 1 and 2 and the Supplementary Information. Extra data are available from the corresponding author upon request. Source data are provided with this paper.

Acknowledgements

This work was supported by the National Natural Science Foundation of China under grant numbers 52021006 (J. Zhang), 52025023 (K.L.) and 51991342 (K.L.); the Key R&D Programme of Guangdong Province with grant numbers 2020B010189001 (K.L.), 2019B010931001 (K.L.) and 2018B030327001 (K.L.); the National Key R&D Programme of China under grant numbers 2016YFA0300903 (K.L.), 2017YFA0303800 (K.L.) and 2016YFA0300804 (P.G.); the Strategic Priority Research Programme of Chinese Academy of Sciences with grant number XDB33000000 (K.L.); Beijing Natural Science Foundation under grant number JQ19004 (K.L.); Beijing Graphene Innovation Programme under grant number Z181100004818003 (K.L.); the Pearl River Talent Recruitment Programme of Guangdong Province with grant number 2019ZT08C321 (K.L.); National Equipment Programme of China under grant number ZDYZ2015-1 (X.B.); National Postdoctoral Programme for Innovative Talents under award number BX20190016 (C.L.) and China Postdoctoral Science Foundation under award numbers 2019M660280 (C.L.) and 2019M660281 (R.Q.).

Author contributions

K.L. conceived and supervised the project. F.Y., Y.S. and H.M. designed and built the optical setup. F.Y., W.Y. and C.L. conducted the optical experiments. C.L. performed sample growth and the scanning tunnelling microscope experiments. Y.S., Y.Y., F.Y., W.Y. and H.M. contributed the theoretical calculations. R.Q., P.G. and X.B. conducted the transmission electron microscopy experiments. C.W., C.M., J. Zhao, Z.S., S.M., F.W. and J. Zhang suggested optical experiments. All of the authors discussed the results and wrote the paper.

Competing interests

The authors declare no competing interests.

Additional information

Extended data are available for this paper at https://doi.org/10.1038/s41565-021-00953-w.

Supplementary information The online version contains supplementary material available at https://doi.org/10.1038/s41565-021-00953-w.

Correspondence and requests for materials should be addressed to K.L.

Peer review information *Nature Nanotechnology* thanks the anonymous reviewers for their contribution to the peer review of this work.

Reprints and permissions information is available at www.nature.com/reprints.

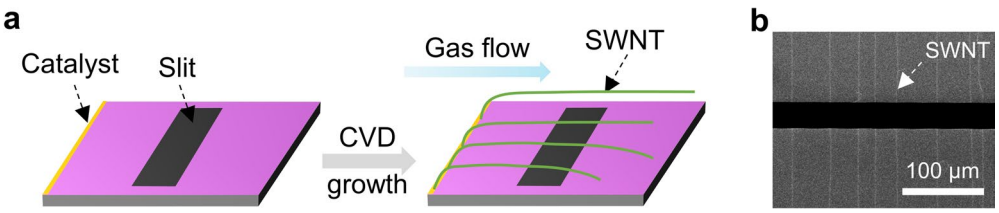

Extended Data Fig. 1 | Synthesis of SWNTs. **a**, Schematic of SWNTs growth across open slit by kite-flying growth mechanism. **b**, SEM image of the as-grown SWNTs.

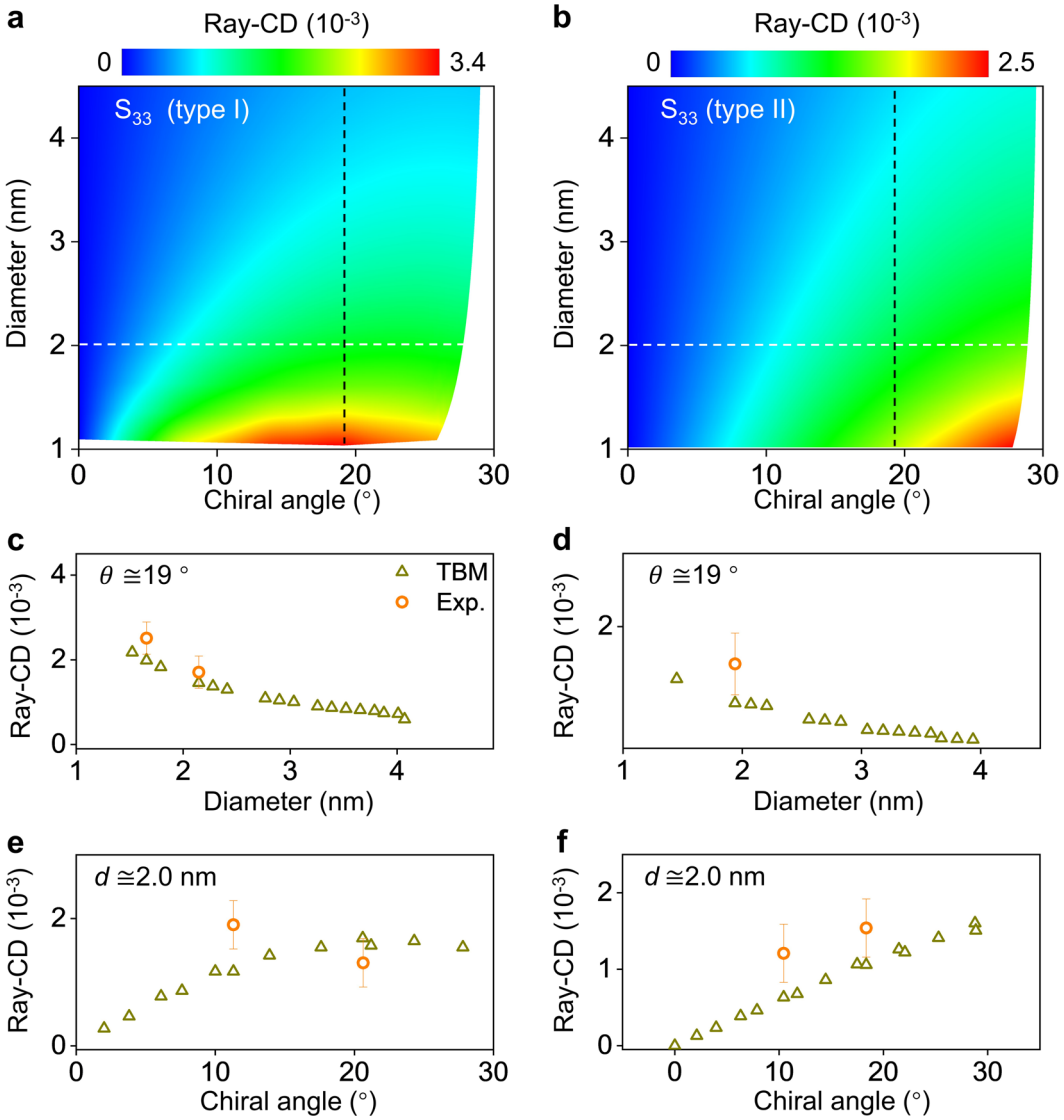

Extended Data Fig. 2 | Structure-dependent Ray-CD peak intensity. a,**b**, Calculated mapping of Ray-CD peak intensity as a function of the diameter and chiral angle of S_{33} transition for semiconducting type I (**a**) and type II (**b**) nanotubes. **c**,**d**, Calculated (green triangles) versus experimental (orange circles) peak intensities of Ray-CD for S_{33} transitions as a function of diameter for type I (**c**) and type II (**d**) family. The chiral angle of selected nanotubes is around 19 ° (black lines in calculated mappings). **e**,**f**, Calculated (green triangles) versus experimental (orange circles) peak intensities of Ray-CD for S_{33} transitions as a function of the chiral angle for type I (**e**) and type II (**f**) family. The diameters of the selected nanotubes are around 2.0 nm (white lines in calculated mappings). Error bars are derived from absolute Ray-CD values of armchair samples.